10.1021/acs.langmuir.2c01019

Gummy Nanoparticles with Glassy Shells in Electrostatic Nanocomposites

Sandrine Lteif[1], Khalil Akkaoui[1], Samir Abou Shaheen[1], Maya Chaaban[1], Steven Weigand[2], and Joseph B. Schlenoff[1*]

[1]Department of Chemistry and Biochemistry, The Florida State University, Tallahassee, Florida 32306, United States, [2]DND-CAT Synchrotron Research Center, Northwestern University, APS/ANL 432-A005, 9700 S. Cass Avenue, Argonne, Illinois 60439, USA

*jschlenoff@fsu.edu

10.1021/acs.langmuir.2c01019

Abstract

Nanocomposites with unusual and superior properties often contain well-dispersed nanoparticles. Polydimethylsiloxane, PDMS, offers a fluidlike or rubbery (when crosslinked) response, which complements the high-modulus nature of inorganic nanofillers. Systems using PDMS as the nanoparticulate, rather than the continuous, phase are rare because it is difficult to make PDMS nanoparticles. Aqueous dispersions of hydrophobic polymer nanoparticles must survive the considerable contrast in hydrophobicity between water and the polymer component. This challenge is often met with a shell of hydrophilic polymer or by adding surfactant. In the present work, two critical advances for making and using aqueous colloidal dispersions of PDMS are reported. First, PDMS nanoparticles with charged amino end groups were prepared by flash nanoprecipitation in aqueous solutions. Adding a negative polyelectrolyte, poly(styrene sulfonate), PSS, endowed the nanoparticles with a glassy shell, stabilizing them against aggregation. Second, when compressed into a nanocomposite, the small amount of PSS leads to a large increase in bulk modulus. X-ray scattering studies revealed the hierarchical nanostructuring within the composite, with a 4 nm PDMS micelle as the smallest unit. This class of nanoparticle and nanocomposite presents a new paradigm for stabilizing liquidlike building blocks for nanomaterials.

Introduction

Tuning the properties of polymer nanocomposites has been of interest in the field of soft functional materials for many years.[1-5] Improving properties such as modulus[6], toughness, and conductivity can be achieved by introducing nanofillers. These nanofillers are usually inorganic such as silica[7-9] and other metal oxides, or gold,[10] or are combined with organic building blocks such as nanocellulose,[11, 12] block copolymers[4] and vitrimers. Specific interactions can occur

between particles and their constituents on the nano scale leading to unique architectures and properties.[1, 2, 13] For example, crosslinked polydimethylsiloxane, PDMS, or “silicone rubber” often contains a dispersion of nanosilica to impart toughness. A wide variety of nanoparticle types offers a broad scope for designing functional nanocomposites with controlled inter-particle ordering.[4] Combining metal-organic frameworks with polymers enhances their processibility. The influence of the polymer network on the viscoelastic properties of polymer nanocomposites has been examined extensively.[4, 14-16]

All-polymer nanocomposites bind dispersions of polymer nanoparticles with other polymers.[8, 17] Water-stable polymer nanoparticles usually have a hydrophobic core and a hydrophilic polymer shell that stabilizes the particles.[13, 18, 19] As a soft polymer, PDMS is a widely-used non-toxic, biocompatible hydrophobic polymer with high thermal resistance, and low glass transition temperature, T_g.[13, 20-22] Unfortunately, there is a strong difference in solubility between PDMS and other common polymers such as polystyrene, poly(methyl methacrylate) or poly(vinyl chloride).[13] Its low T_g, beneficial for use in elastomeric products, means PDMS remains liquid-like at room temperature. Thus, pure PDMS nanoparticles, even when cross-linked, are inclined to fuse during preparation.[21] The synthesis of stable, PDMS nanoparticles is consequently challenging. To address this problem, researchers have incorporated PDMS within block copolymers[20, 23] or modified the surface with hydroxyl groups.[21, 22] Recently, montmorillonite[24] and polystyrene[25, 26] have been incorporated to toughen PDMS.

Because PDMS is exceptionally hydrophobic it can sequester various hydrophobic compounds, such as pharmaceuticals, from water, which offers great potential in biomedical and material science applications.[20, 23, 27] For the same reason, PDMS is widely used in strategies for environmental remediation of organics, such as encapsulating nanocatalysts to destroy contaminants,[28] or in membranes for separating oil from water.[29] A high specific surface area that

is offered by nanoparticles accelerates the sorption of hydrophobic molecules from aqueous solutions.

Composite polysiloxane dispersions are predominantly made by first polymerizing siloxane monomers to form a core and then adding monomers with vinyl groups to graft on a shell.[13] Alternatively, PDMS-containing block copolymers can self-assemble in selective solvents. Various factors affect this self-assembly such as polymer concentration, molecular weight, volume ratio of the segments and the chemical nature of the hydrophobic and hydrophilic blocks.[23] pH-dependent spherical polydimethylsiloxane/poly(2-(dimethylaminoethyl acrylate) charged micelles were prepared by Zhao et al.[20] Micelle formation was examined using 1-naphthylamine (PNA) as a probe that exhibited a large blue shift of λ_{max} and enhanced fluorescent intensity when solubilized in the hydrophobic core.[20] Maparu et al. have created soft PDMS nanoparticles modified by hydroxyl groups that form intramolecular hydrogen bonds thus improving the PDMS surface energy and mechanical strength.[21]

In the present work, the difficult problem of stabilizing PDMS nanoparticles, especially in aqueous environments, has been addressed with the addition of a glassy electrostatic shell of polyelectrolyte complexed to charged groups on the ends of the PDMS chains. This shell provides aqueous dispersions of PDMS nanoparticles which are stable even with the addition of salt. When compressed, the charged polymer electrostatically stitches together PDMS nanoparticles to provide a unique, toughened, hierarchical structure which was elucidated with x-ray scattering studies.

Results and Discussion

Nanoparticle dispersions were prepared by rapidly mixing low molecular weight PDMS dissolved in THF with a large volume of water (nonsolvent).[30] Flash nanoprecipitation (FNP) yielded reproducible particles in the range of 40 – 65 nm by controlling the mixing rate and solvent

ratio. Particle nucleation is induced by local supersaturation in a turbulent regime in a confined volume.[30-33] Flash nanoprecipitation was investigated by Prud'homme and coworkers[30, 32, 34] using confined impinging jets (CIJ) mixers. Impinging jets, which deliver rapid mixing times, have been used to prepare polymer nanoparticles that encapsulate inorganic and pharmaceutical agents.[30, 32, 33] The CIJ used here was adapted from an optimized geometry reported by Han et al.[31]

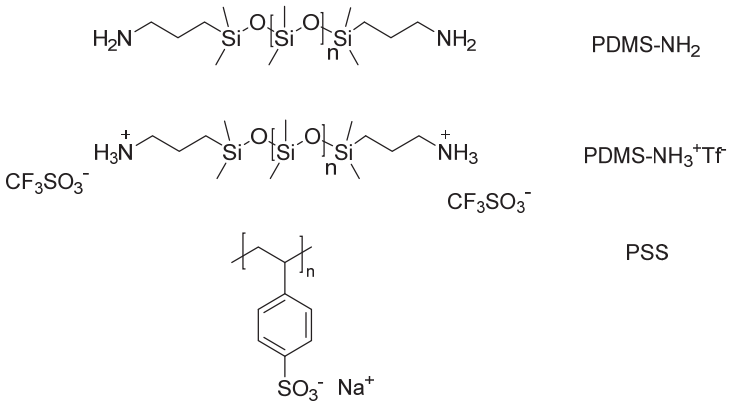

Scheme 1. Structures of polymers used.

Positively charged nanoparticle. The starting PDMS (PDMS-NH_2, Scheme 1) had a flexible hydrophobic siloxane backbone (T_g about -123 ^oC[21]) with amine end groups. This commercially available polymer has a nominal molecular weight of about 900 g mol^{-1}, yielding a low viscosity of about 10-15 cST. In order to stabilize the aqueous nanodispersion by electrostatic repulsion, PDMS-NH_2 was charged by protonating the end groups. To provide solubility in organic solvents, triflic acid was used, leaving the hydrophobic triflate as a counterion. The protonated product (PDMS-$NH_3^+Tf^-$, Scheme 1) was characterized by ^1H NMR spectroscopy. End groups were assigned using COSY (see Supporting Information Figures S1 and S2) and the PDMS was determined to have an average of 17 repeat units (Figure S3, M_n = 1375 g mol^{-1}). When crosslinked, PDMS is an elastomer that has been used in numerous industrial and biomedical applications due to its chemical inertness and biocompatibility.

10.1021/acs.langmuir.2c01019

The liquidlike nature of PDMS, combined with its intense hydrophobicity, thwarts attempts to produce stable dispersions of PDMS nanoparticles. The few reports of such materials [20, 21, 23, 35] rely on a couple of strategies for stabilization, including the classical method of adding surfactant.[36] Internal crosslinking removes the liquidlike nature of PDMS,[21] while incorporating a PDMS block along with a hydrophilic block in copolymers yields micelles stabilized by a hydrophilic corona.[20, 23]

Rapid supersaturation, precipitation, and dilution tend to yield small, stable polymer nanoparticles.[30, 31] The mixer was designed to provide these conditions (Figure S4, Supporting Information). The polymer solution and non-solvent (water) emerge from two opposing outlets into a small mixing chamber with a residence time of about 0.2 mS under turbulent flow. The nanoparticles were immediately ejected into a large reservoir of water (Figure S5, Supporting Information). The PDMS nanoparticles obtained in the reservoir had a hydrodynamic radius, R_h, of 53 nm determined by dynamic light scattering (DLS, Figure 1) and remained stable in size for

at least 24 h (see Figure S6 Supporting Information). Particle size distributions were reasonably narrow (Figure 1) and the R_h was reproducible from run to run within ± 3 nm.

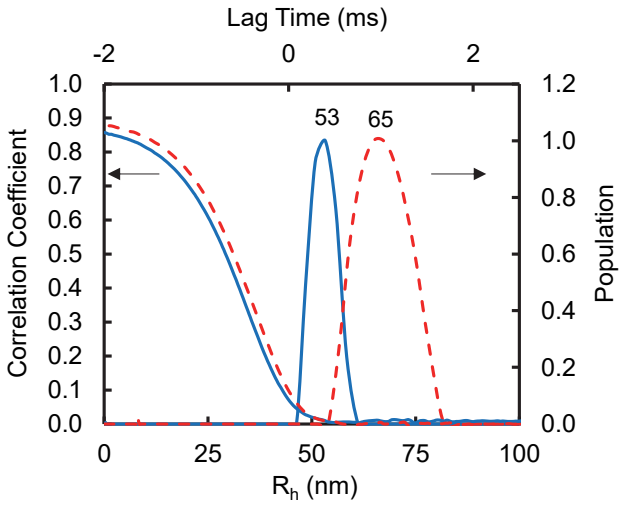

Figure 1. Autocorrelation function and hydrodynamic radius, R_h, distribution of 1 mg mL^{-1} PDMS-$NH_3^+Tf^-$ nanoparticles at an angle of 90º at 296.8 K (—); and PDMS-NH_3^+PSS (--) as made in water. R_h remains essentially unchanged after 24 h (see Supporting Information Figure S6).

Colloidal stability was presumed to be provided *via* electrostatic repulsions between positively charged nanoparticle surfaces.[37] This classical mechanism was supported by the finding that the nanoparticle dispersion destabilized on the addition of salt.[38] For example, when 0.15 M NaCl was introduced to the nanoparticle reservoir an increase in hydrodynamic radius was recorded over the course of 8 hours (Figure 2). A higher salt concentration induced faster nanoparticle aggregation.

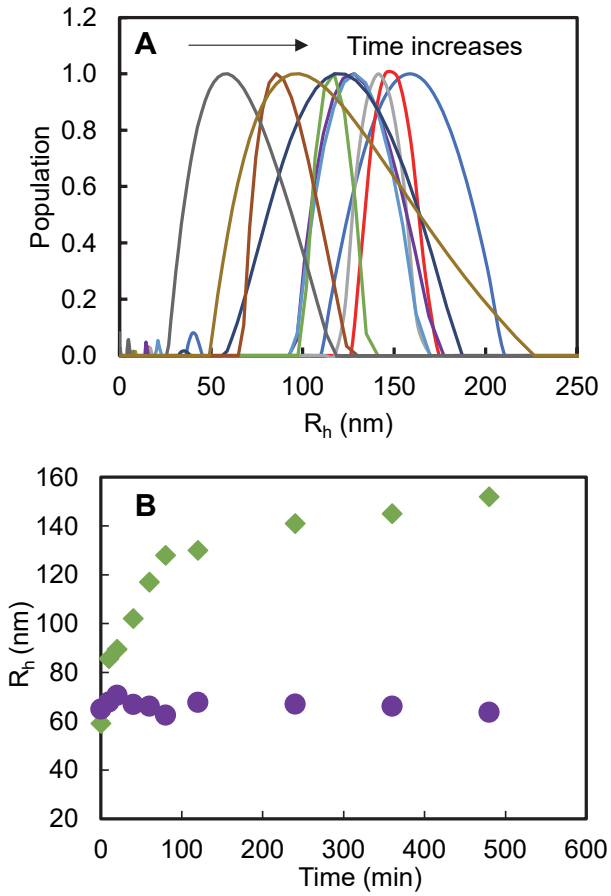

Figure 2. (**A**) Hydrodynamic radius distribution of 1 mg mL^{-1} PDMS-$NH_3^+Tf^-$ nanoparticle in 0.15 M NaCl at an angle of 90º at 296.8 K; (**B**) R_h of 1 mg mL^{-1} PDMS-$NH_3^+Tf^-$ nanoparticle (♦) and PDMS-NH_3^+PSS nanoparticles (●) in 0.15 M NaCl versus time

PDMS-$NH_3^+Tf^-$ nanoparticles were deposited on silicon wafer primed with a 1 nm bilayer of poly(diallyldimethylammonium) and poly(styrene sulfonate) (PDADMA/PSS), which has a negative surface charge. An AFM image (Figure 3A) of the nanoparticle layer shows rings of linear aggregates of smaller particles forming a larger aggregated structure of the PDMS-$NH_3^+Tf^-$, similar to patterns produced by complexed silica nanoparticle composites.[39] Several line scans similar to the one depicted in Figure 3B were used to determine the height distributions of the

particles making up the linear aggregates. The height of the particles is assumed to be the size of the smallest unit (micelle) discussed below, with a diameter of 4 to 8 nm (Figure 3C).

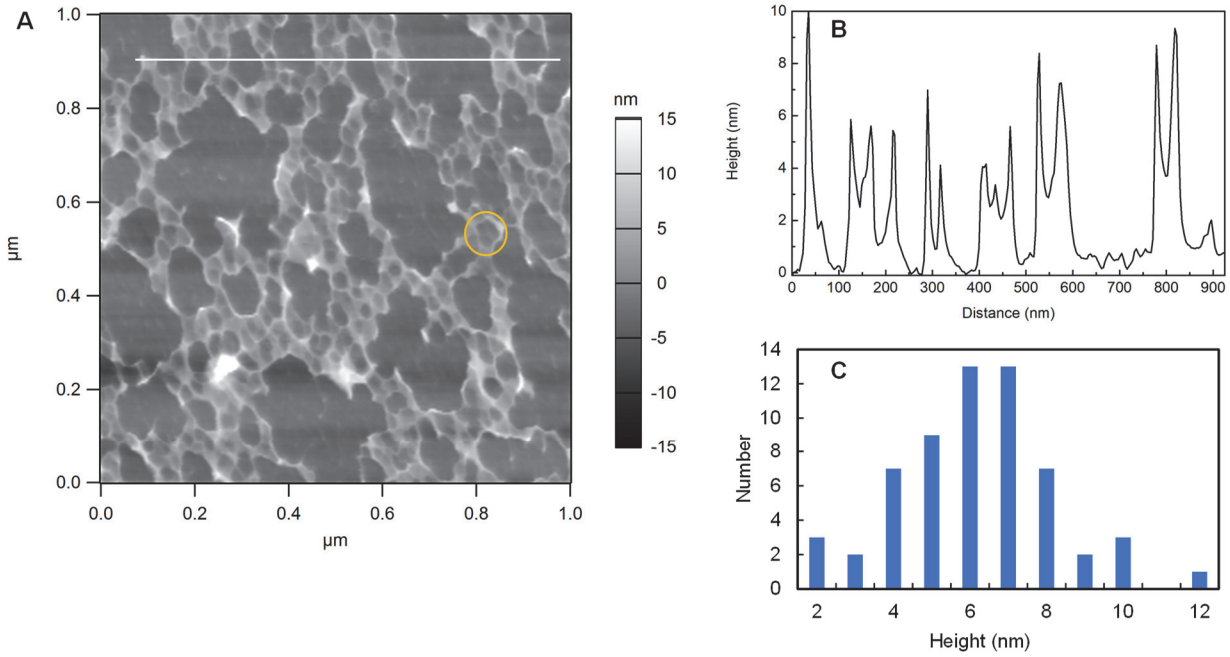

Figure 3. (**A**) AFM image of PDMS-$NH_3^+Tf^-$ nanoparticles deposited on a PDADMA/PSS bilayer. X-Y scales are 1 x 1 μm. Yellow circle indicates a radius of 50 nm. (**B**) Height profile along white line in image A. (**C**) Height distribution histogram of the maxima along line scans.

Positively charged nanoparticle with a glassy PSS shell. Nanoparticles are used in many environments having significant ionic content capable of promoting aggregation of the type seen in Figure 2. Of particular interest are physiological environments, which have a salt concentration close to that used in Figure 2. To enhance the stability of the nanoparticles, a PSS shell was introduced on their surface. PSS was added to the receiving reservoir of the FNP reactor. The

PDMS-NH_3^+ PSS nanoparticle hydrodynamic radius increased slightly compared to the positively charged nanoparticle (Figure 1).

Several experiments were directed towards optimizing the ratio of PSS^-:PDMS-NH_3^+ charges with the objective of minimizing the amount of PSS needed, maintaining R_h around 50 nm, and preserving stability in salt solutions (see Supporting Information Figures S7 to S9 for summaries). It was found that an excess of PSS was required, optimized to a PSS^-:PDMS-NH_3^+ charge ratio of 2:1. Because of this, excess PSS (about 0.04 mM) remained in the FNP reservoir after nanoparticle precipitation. Longer PSS chains (e.g. 45,000 g mol^{-1}) led to larger nanoparticles, presumably because bridging interactions came into play. The PSS shell enhanced the stability of the nanoparticle, keeping the R_h constant in 0.15 M NaCl (Figure 2B).

Inorganic nanoparticles are often stabilized with a layer of adsorbed polyelectrolyte.[40] Given both the liquidlike nature and hydrophobicity of short PDMS, it was surprising to find strong stabilization of the nanoparticles formed here with approximately (or less than) one layer of PSS. It is believed the electrostatic complex formed between -NH_3^+ end groups and styrene sulfonate repeat units had a glassy nature. A hydrated complex between a primary polyamine and PSS was found to have a glass transition temperature of 60 to 90 ^oC.[41] Capsules with walls of ultrathin polyelectrolyte complex[42] show the same T_g as bulk complexes of the same material.[41] Additional evidence for a substantial increase in stiffness is given below.

PDMS-NH_3^+PSS Composite. Solid PDMS-NH_3^+PSS was prepared by centrifuging a PDMS-NH_3^+PSS nanoparticle solution. This operation allowed for the measurement of PSS in the complex versus excess PSS left in solution using UV-Vis absorption spectroscopy (Supporting Information Figure S10) of the PSS remaining in the supernatant. The charge ratio of PDMS-NH_3^+:PSS^- in the complex was about 2:1 (the presence of excess triflate to balance the charge was supported by FTIR, see Supporting Information Figure S11). Though the viscoelastic responses (VR) of bulk unprotonated and protonated PDMS starting material were similar, the

VR of solid protonated polysiloxane was drastically altered with the inclusion of a small amount of PSS.

The storage modulus G', loss modulus G'', (Figure 4A) and viscosity (Figure S12, Supporting Information) increased more than 100-fold in the dry material when 14 wt% PSS was incorporated in the nanomaterial. Both G' and G" remained high when the composite was heated to 150 °C with no evidence of a glass transition in this temperature range (Figure 4). The dependence of VR on temperature was reversible (see heating and cooling curves in Figure 4B). In comparison, some nanocomposites with inorganic nanofillers show temperature irreversible viscoelastic behavior.[43]

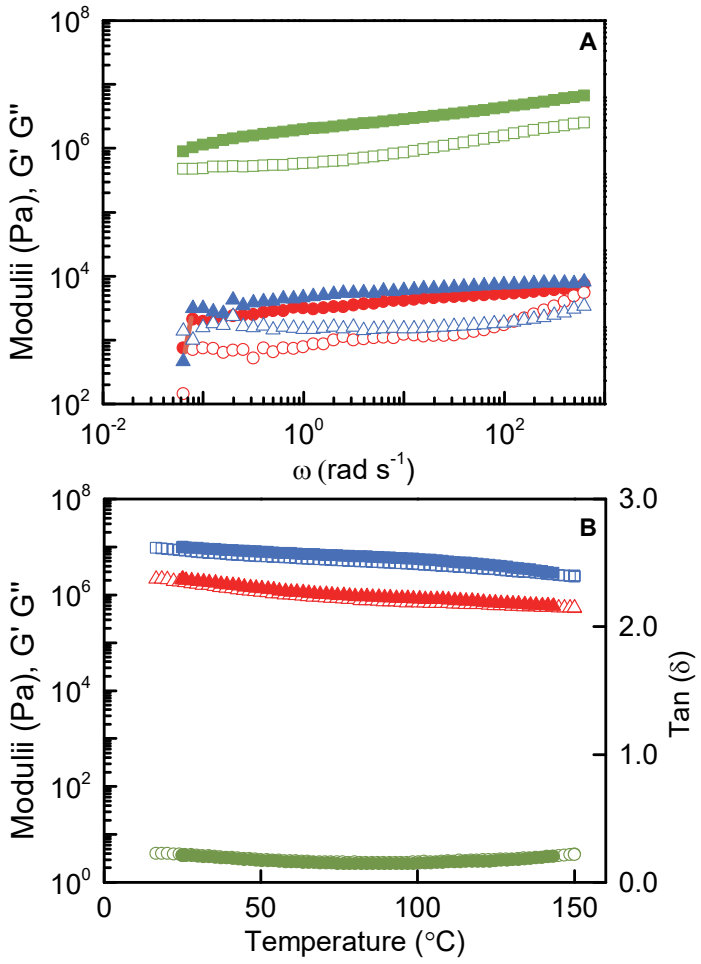

Figure 4. (**A**) Linear viscoelastic response (G' filled, G'' open symbols) of PDMS-NH_3^+PSS nanocomposite (green squares), bulk PDMS-$NH_3^+Tf^-$ (blue triangles) and PDMS-NH_2 at 25 ^oC (red circles); (**B**) VR at 0.1% strain 1 Hz frequency while ramping temperature at 1 ^oC min^{-1} for PDMS-NH_3^+PSS. Storage modulus (G', heating□, cooling ■), loss modulus (G", heating Δ, cooling ▲) and tanδ (heating ○, cooling ●).

PSS itself is glassy and shows no evidence of a T_g up to 250 ^oC.[41] Glassy neutral polymers such as polystyrene (T_g ≈ 100 ^oC) have been used to improve the mechanical properties of PDMS.[26] The styrene monomer was either incorporated by *in situ* polymerization in a PDMS matrix[25] or by the formation of a block copolymer.[26]

The effect and mechanism of a mere 14 wt % PSS on the VR of this nanocomposite are reminiscent of enhanced stiffness of neutral polymers induced by including a few percent of charged units. These materials, falling under the broad definition of ionomers, are used and investigated widely.[44] For example, introducing 2.5 mol% of styrene sulfonate increased the melt viscosity of polystyrene by about three orders of magnitude.[45] The ionic units cluster into regions which act as crosslinks. A model by Eisenberg et al. invoking clusters of ionic groups[46] was to explain the SAXS of some ionomers.[47] Viscoelastic properties also depend on the nature of the counterions, which are trapped within these clusters.[45, 48] The nanocomposite prepared here differs in that half of the charge is balanced by triflate ions and half by PSS, which presumably bridge aggregated nanoparticles. The modulus of PDMS-NH_2 increases only slightly on the introduction of charge, whereas the polymeric counterion PSS leads to dramatically higher modulus, which is seen by comparing the VR of unprotonated and protonated PDMS-NH_2 in Figure 4B. Thus, molecular crosslinking via electrostatic charge pairs between -NH_3^+ and sulfonates must be essential for the enhanced modulus.

Structure from X-ray Scattering. X-ray scattering was used to understand the morphology of the PDMS-NH_3^+PSS nanoparticles in solution and the nanocomposite. The detectors were

designed to acquire small, mid and wide-angle x-ray scattering on the same sample, allowing for structural analysis over many length scales.[49]

Bulk PDMS-NH_2 and PDMS-$NH_3^+Tf^-$. Comparing the x-ray scattering of the bulk PDMS-NH_2 starting material and the protonated PDMS-$NH_3^+Tf^-$, a distinct new peak appeared at q = 0.266 $Å^{-1}$ with a Porod slope of -4 indicating a spherical nanoparticle (micelle) of PDMS-$NH_3^+Tf^-$ with a radius of about 12 Å (Figure 5 and Figure S14C). A PDMS-$NH_3^+Tf^-$ dispersion in water was not stable when a concentrated solution was prepared for x-ray scattering. A PDMS-NH_3^+PSS nanoparticle dispersion in water was prepared, filtered through a 0.1 μm filter, and concentrated to 10 mg mL^{-1}. The size of the nanoparticles in the more concentrated solution was the same as in dilute solutions and remained stable (verified by DLS). The scattering profile of the PDMS-NH_3^+PSS dispersion (Figure 5) includes residual scattering from solution PSS between 0.018 and 0.275 $Å^{-1}$ which overwhelms the profile. The scattering profile of PSS in solution (Figure S15) shows the characteristic broad “polyelectrolyte” peak.[50] This excess solution PSS is absent in the scattering profile of the nanocomposite. The broad shoulder at 0.114 $Å^{-1}$ in the solution PDMS-NH_3^+PSS profile (Figure 5) is probably due to correlations between particles separated by 32 Å.

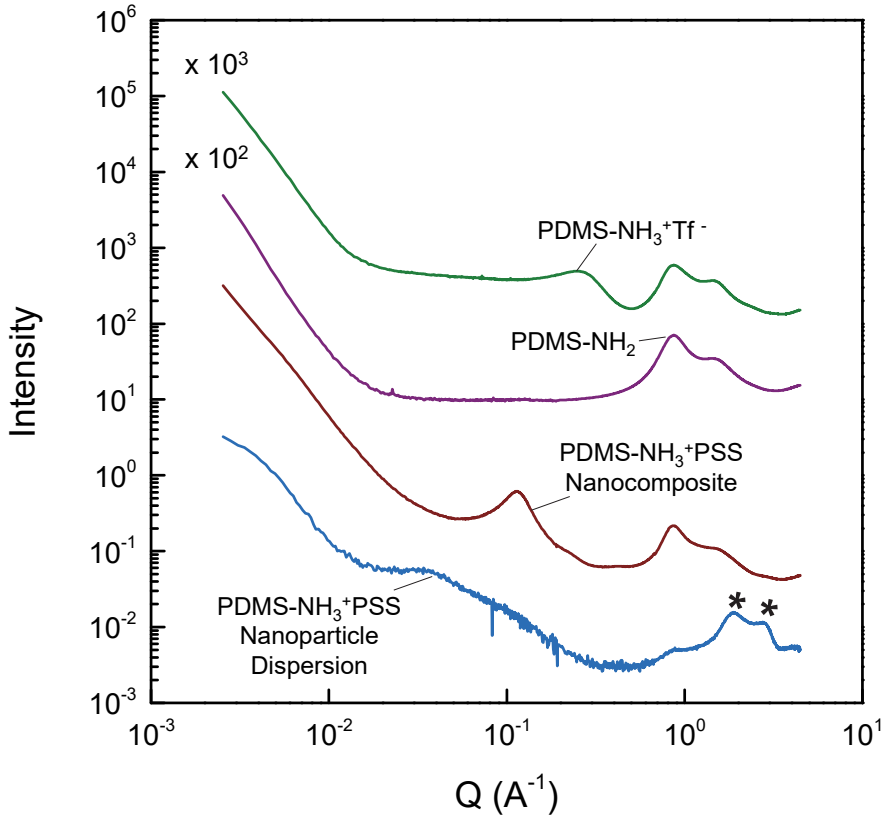

Figure 5. Small-, mid- and wide-angle x-ray scattering profiles of bulk PDMS-$NH_3^+Tf^-$, bulk PDMS-NH_2, bulk PDMS-NH_3^+PSS nanocomposite, and PDMS-NH_3^+PSS 1 wt% nanoparticle dispersion (top to bottom). PDMS-NH_2 and PDMS-$NH_3^+Tf^-$ curves are shifted upwards for clarity. Both of these materials show scattering characteristic of mass fractals at low Q. *Peaks at 1.75 $Å^{-1}$ and 2.77 $Å^{-1}$ in the PDMS-NH_3^+PSS 1 wt% nanoparticle dispersion profile are from water (Figure S13).

The scattering of PDMS-NH_3^+PSS as a dispersion and as a solid were analyzed using a unified Guinier exponential and Porod law fit that provides characteristic R_gs and shapes.[51, 52] Figure 6 shows the small angle scattering (SAXS) profiles of PDMS-NH_3^+PSS nanoparticle dispersion and PDMS-NH_3^+PSS solid with three and two populations of scattering features with characteristic sizes, respectively.

PDMS-NH_3^+PSS nanoparticle dispersion in water

Population **I** in Figure 6A is modeled by a mass fractal with power law slope of about -2 made of aggregates of primary particles.[53, 54] This mass fractal has a R_g of 440 Å that is slightly smaller than the hydrodynamic radius for the PDMS-NH_3^+PSS nanoparticle (Figure 1). At q = 0.018 $Å^{-1}$ population **II** starts to govern the scattering profile. Population **II** was attributed to excess solution PSS remaining from the FNP, with an R_g of 89 Å, reasonable for 16,000 g mol^{-1} molecular weight PSS (Figure S14A). The slope of -2 is from the Gaussian coil of the solution polyelectrolyte (Figure S15).[54, 55] The R_g = 32 Å substructure of population **III** with a power law of -4 corresponds (Figure S14A) to a spherical shape for the primary nanoparticle[53] of PDMS-$NH_3^+Tf^-$ micelles. A PDMS-NH_3^+PSS network with spherical substructure was seen using AFM when PDMS-NH_3^+PSS nanoparticles were deposited on a PDADMA/PSS/PDADMA tri-layer (having a positively charged surface) on silicon wafer (Figure S16).

PDMS-NH_3^+PSS nanocomposite

In the PDMS-NH_3^+PSS nanocomposite (Figure 6B), the mass fractal becomes a surface fractal with a power slope of -3.[53]. A dense spherical micellar substructure takes over the profile at 0.078 $Å^{-1}$, with a peak at 0.108 $Å^{-1}$ corresponding to an R_g of 21 Å and a power slope of -4. The slight decrease in size compared to the 32 Å feature in Figure 6A could be due to shrinkage of the PDMS/PSS shell when the nanocomposite was dried and the fact that shorter correlation distances are observed at high concentrations.[56]

10.1021/acs.langmuir.2c01019

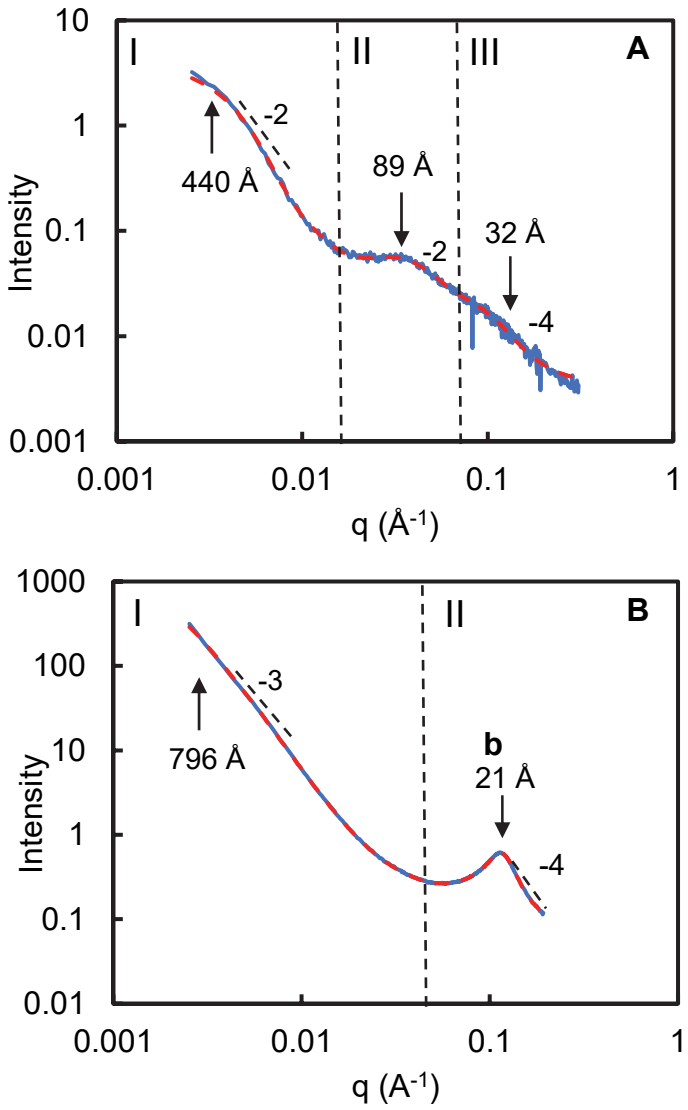

Figure 6. SAXS profile (—) and unified fit model (--) of (**A**) PDMS-NH_3^+PSS 1 wt% nanoparticle dispersion in water and (**B**) PDMS-NH_3^+PSS nanocomposite with distance "**b**" corresponding to

the R_g of the smallest subunit. The individual fits for population **I**, **II** and **III** are broken out in Supplementary Figure S14 (A-B).

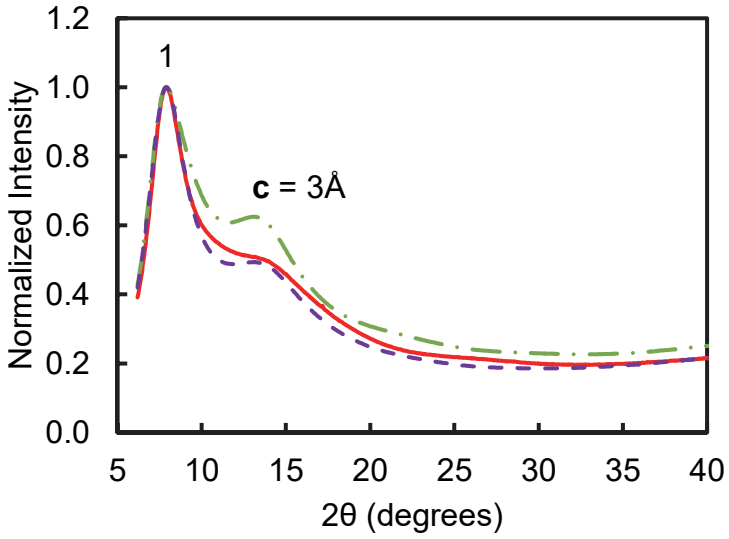

Figure 7. Wide angle scattering (WAXS) profile PDMS-NH_3^+PSS nanocomposite (—), PDMS-$NH_3^+Tf^-$ (-·-) and PDMS-NH_2 (--) with peak 1 as the amorphous halo of PDMS[57] and peak "**c**" as distance between the ammonium end groups

In solution, the interferences between loosely aggregated nanoparticles can be ignored due to large distances separating them.[58] The loosely aggregated nanoparticles in solution compress together in the nanocomposite. For the nanocomposite, a structure factor was needed to describe intermicellar correlations which are correlated by a distance of 133 Å (see Scheme 2). 49 Å in population **II** represents the mean distance between two positively charged micelles held together with PSS (Scheme 2). The WAXS profile in Figure 7 shows the amorphous halo of PDMS at 7.86º[57] (Peak 1) which remains at the same position for the different PDMS samples showing that the amorphous nature of the PDMS is unchanged in the composite.[57] Peak **c** at 13.2º represents the distance between non-PDMS segments. This means that the distance between the two -NH_3^+ end groups would be around 3 Å (Scheme 2). When combining the

information obtained from x-ray scattering, a suggested micellar network can be sketched (Scheme 2). Scheme 2A represents the dispersed R_g = 440 Å aggregates of solution PDMS-NH_3^+PSS nanoparticles. Without the stabilizing shell of PSS, similar PDMS-$NH_3^+Tf^-$ aggregates fuse into larger aggregates when deposited on Si wafer (Figure 3). Scheme 2 depicts all the length scales, including the correlation between micelles in the nanocomposite (**a**) and compressed clusters of micelles (**d**), the approximate average contour length of the PDMS block, the R_g of micelle cores (**b**) and the separation between micelle cores (**c**) that includes a PSS chain.

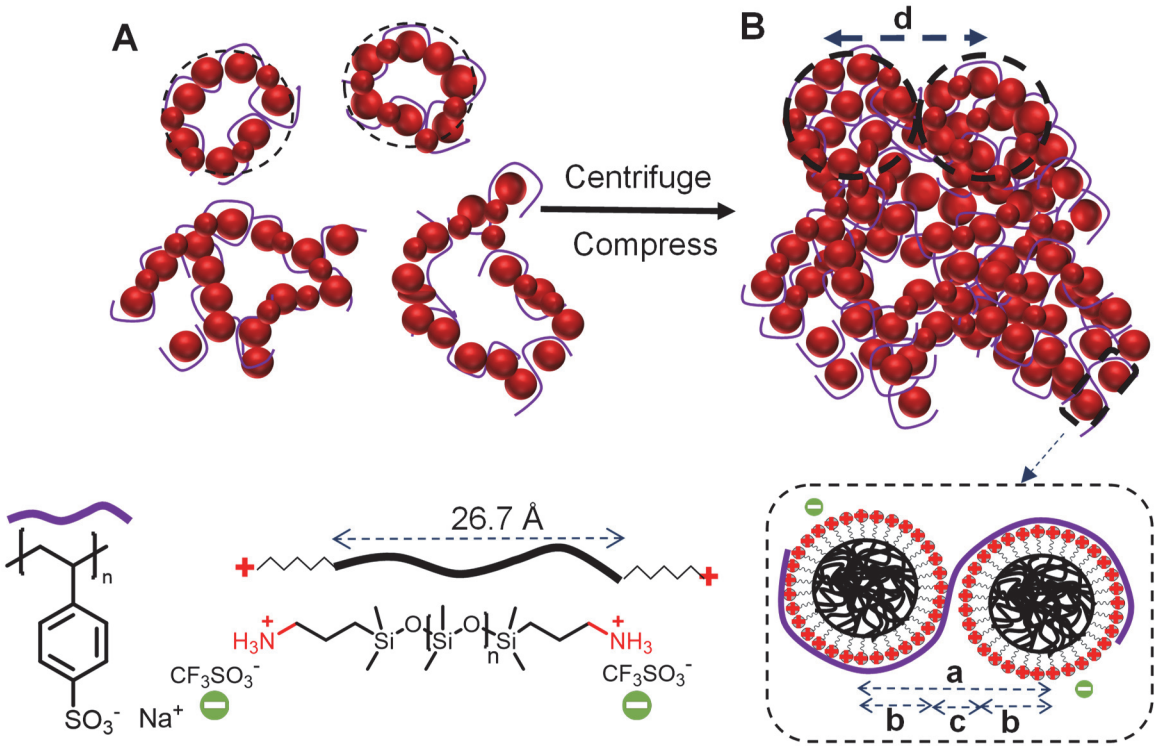

Scheme 2. Scheme of (**A**) PDMS-NH_3^+PSS nanoparticle dispersion, the primary particle (micelles, red sphere) and the aggregates of the primary particle (dashed circle) connected by PSS bridges and (**B**) the nanocomposite network with agglomerates of aggregates connected by PSS bridges. The PSS chain has a contour length of about 130 Å. 133 Å describes the correlation inside a larger aggregated fractal between the agglomerates of aggregates. The strong correlation between the primary particles with a short distance (48.5 Å) represented by abutting spheres. The

contour length of 17 siloxane repeat units is 26.7 Å, estimated by an MM2 computational method after energy minimization of the PDMS structure. Distances "**a**" (48.5 Å, Table S1), "**b**" (21 Å, Figure 6B) and "**d**" (133 Å, Table S1) in the nanocomposite are deduced by SAXS. Distance "**c**" (3 Å, Figure 7) is determined by WAXS.

PDMS nanoparticles as hydrophobic nanocarriers

PDMS particles that are stable at physiological salt concentrations, shown in Figure 2, might have applications as carriers of hydrophobic molecules such as water-insoluble pharmaceuticals.[21] To demonstrate such a potential application, nanoparticles of PDMS-NH_3^+PSS were used to absorb a 3-hydroxychromone derivative, 2-(furan-2-yl)-3-hydroxy-4H-chromen-4-one (FG38).[59] In nonpolar media, FG38 emits light from a tautomeric (T*) state at 543 nm *via* excited-state intramolecular proton transfer (ESIPT). In polar media, normal emission at 430 nm is preferred (N*).[60] The PDMS-NH_3^+PSS nanocomposite was dipped in a 5 x 10^{-6} M solution of FG38 in water and the absorbance of the dye was monitored using UV-Vis spectroscopy (Figure S17). The absorbance of FG38 in water gradually decreased (Figure S18) indicating the diffusion of the dye into the nanocomposite. Figure 8 displays the two bands corresponding to emission from N* and T* states in water and in the nanocomposite. The increase of emission from the T* state in the nanocomposite shows that the photophysics responds to the more nonpolar environment of the PDMS. Emission decay lifetime measurements of FG38 in the PDMS-NH_3^+PSS nanocomposite show a slower decay for the T* emission (Figure S19). The T* emission follows biexponential kinetics (decay time for the fast component 5 ns, Table S2) while N* is characterized by a nearly mono-exponential fast decay (lifetime of 2 ns Table S2). (With a negligible amplitude of the long-lived decay component A_2 and t_2).[59]

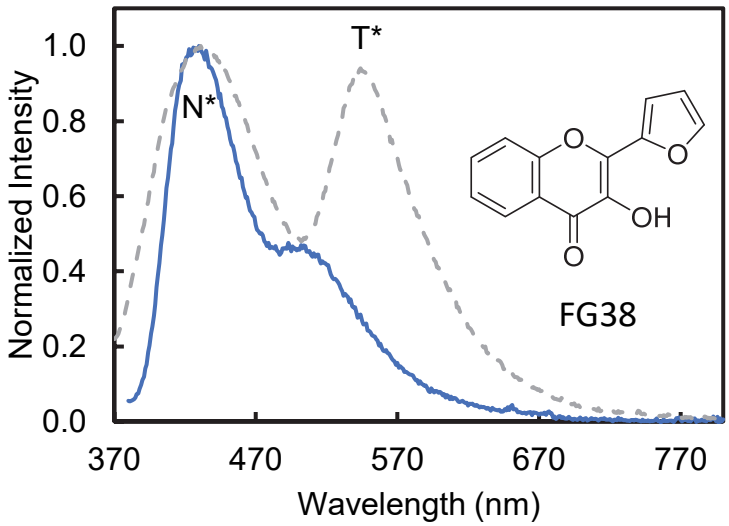

Figure 8. Emission profile of FG38 in water (blue) and in PDMS-NH_3^+PSS nanocomposite (dashed, grey).

Conclusions

A straightforward method to prepare building blocks for nanomaterials from liquid-like, hydrophobic components has been described. Short PDMS chains usually have low viscosity and tend to fuse in polar environments. Using flash nanoprecipitation, amine-terminated PDMS nanoparticles were capped with a glassy polyelectrolyte shell. During precipitation, micellar subunits PDMS, R_g of 3 nm, clustered together to form larger diameter fractals of R_g = 44 nm. These nanoparticles were stable in saline despite the large contrast in polarity between PDMS and water. The nanoparticles could be further compressed to yield a thermally stable nanocomposite of modulus > 10^6 Pa. Detailed SAXS studies showed that the PDMS micelles were preserved and compacted, with the polyelectrolyte serving to bind the micelles together. The duo of stabilized PDMS nanoparticles and nanocomposites made from them offer a new route to

biocompatible, hydrophobic materials with potential applications in separations, drug delivery and encapsulating water-sensitive or insoluble molecules.

Materials and Methods

Materials. Chloroform, sodium chloride (NaCl) and triflic acid were from Sigma Aldrich. Deuterated chloroform ($CDCl_3$) was obtained from Cambridge Isotope Laboratories. Ethanol and HPLC grade water were from VWR Chemicals. Magnesium sulfate anhydrous was from Fisher Scientific. PDADMA was from Alfa Aesar. Aminopropyl terminated polydimethylsiloxane (10-15 cST nominal molecular weight) (PDMS-NH_2) were obtained from Gelest and PSS (16,000 g mol^{-1}, M_w/M_n = 1.07, and 45,000 g mol^{-1} M_w/M_n = 1.02) was from Scientific Polymer Products.

Protonation of PDMS-NH_2 (Scheme 3). 10 g (0.012 mol) PDMS-NH_2 was treated with 2 mL (0.024 mol) triflic acid in 120 mL ethanol at room temperature under N_2 for 8 h (Scheme 1). Ethanol was then removed under reduced pressure. The crude product was dissolved in 120 mL chloroform and washed twice with water (1:1 $CHCl_3$:water). The organic layer was dried using anhydrous magnesium sulfate. The purified product was recovered from the chloroform layer under reduced pressure. PDMS-$NH_3^+Tf^-$ (70% yield) was characterized using COSY and ^{1}H-NMR in $CDCl_3$ (Figures S2 and S3). The number average molecular weight M_n was determined to be 1375 g mol^{-1}. ^{1}H NMR (600 MHz, chloroform-*d*) δ 6.82 (s, 6H), 3.03 – 2.92 (m, 4H), 1.76 – 1.63 (m, 4H), 0.59 – 0.53 (m, 4H), 0.18 – 0.01 (m, 117H).

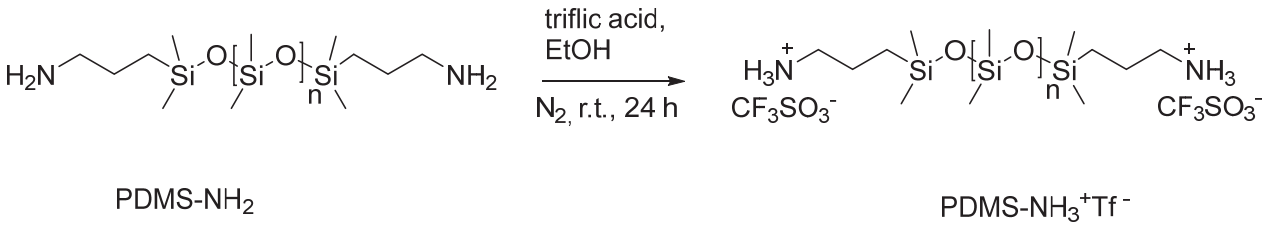

Scheme 3. Protonation of PDMS-NH_2

Nanoparticle Preparation. Flash nanoprecipitation was performed using a hand-operated confined impinging jet dilution (CIJ-D) mixer which was based on a modified literature design (Figure S4).[31] 50 mg of PDMS-$NH_3^+Tf^-$ was dissolved in 2.5 mL of THF and transferred to syringe A, while syringe B had the same volume of water (non-solvent). The syringes were depressed simultaneously to rapidly mix the polymer and the non-solvent. The effluent from the CIJ-D mixer was then instantly diluted in excess (45 mL) water to obtain a THF:water ratio of 5:95 (Figure S5). The total precipitation occurred over a period of 2 s. To form the PSS shell, 30 mg of PSS was dissolved in the 45 mL water, other parameters remaining the same. PDMS concentrations and mixing rates were optimized to avoid the formation of large, polydisperse, unstable particles.

Dynamic Light Scattering (DLS). The size and stability of the nanoparticles were determined using a goniometer light scattering system (ALV CGS-3-A0-111) equipped with a vertically polarized He-Ne laser (λ = 632.8 nm, 22 mW). Measurements were taken, once the sample was prepared at t = 0 and after 24 h, in 10 mm capped borosilicate glass tubes at an angle of 90^o at room temperature through a reservoir filled with a refractive index matching liquid (toluene). The aqueous nanoparticle samples, filtered through a 0.1 μm Millipore filter, had a PDMS-$NH_3^+Tf^-$ concentration of 1 mg mL^{-1}. PSS of molecular weight 16 000 g mol^{-1} and 45 000 g mol^{-1} were used to determine the effect of molecular weight over the concentration range from 0 mg mL^{-1} to 1.2 mg mL^{-1}. The stability in NaCl was monitored over 8 h by adding 75 μL of 4 M NaCl (filtered through a 0.1 μm filter) to 2 mL samples in water. The intensity autocorrelation function $g^{(2)}(q,\tau)$ where $q = 4\pi n_D \sin(\theta/2)/\lambda$ was obtained by pseudo-cross-correlation of the signals from an avalanche photodiode using ALV correlator software V.3.0. The hydrodynamic radius R_h was calculated along with its distribution.

PDMS-NH_3^+PSS Nanocomposite. PDMS-NH_3^+PSS nanoparticle solutions were prepared as above. The dispersion was centrifuged using a Sorvall centrifuge at 10000 rpm for 4 h. The PSS concentration remaining in the supernatant was determined using the absorbance, measured with

a UV-Vis spectrometer (Cary 100 Bio; Varian Instruments) at 225 nm. The precipitate was washed with 10 mL of water and dried under reduced pressure at room temperature. The PSS and PDMS-NH_3^+ content in the nanocomposite were determined to have a 1:1 mole ratio (1:2 charge ratio, Supporting Information Figure S10). The presence of residual Tf^- counterions required to balance the excess PDMS-NH_3^+ in the nanocomposite was confirmed by attenuated total reflection-Fourier transform infrared (ATR-FTIR) spectroscopy using a ThermoScientific Nicolet iS20 with a Pike MIRacle universal ATR attachment fitted with a single-reflection diamond/ZnSe crystal and a high-pressure clamp. The PDMS-NH_3^+PSS nanocomposite spectra (Supporting Information Figure S11) was compared to spectra of PSS, PDMS-NH_2 and PDMS-$NH_3^+Tf^-$ and triflate ion was detected.

Imaging. PDMS-$NH_3^+Tf^-$ nanoparticles (0.1 mg mL^{-1}) were deposited on a PDADMA/PSS bilayer [61] and imaged using an MFP-3D AFM (Asylum Research Inc.) with an ARC2 controller and silicon TESPA-V2 probes (Bruker, radius = 10 nm, spring constant = 42 N m^{-1}). The AC mode (intermittent contact) was employed, and the cantilever was adjusted to 5% below its resonance frequency.

Rheology. The linear viscoelastic responses of the PDMS-NH_3^+PSS nanocomposite, the PDMS-$NH_3^+Tf^-$ polymer and the PDMS- NH_2 starting material were measured using a strain-controlled DHR-3 rheometer with 8 mm and 40 mm parallel plates, respectively. A temperature sweep from 10 to 150 ^oC was performed on the PDMS-NH_3^+PSS nanocomposite at 0.1% strain and a ramp rate of 1 ^oC min^{-1}. Samples were annealed with an initial heating/cooling cycle before data collection. Frequency sweeps were performed from 0.01 to 100 Hz, with a strain of 0.1% at 25 ^oC. The selected strain was verified to be within the linear viscoelastic regime using amplitude sweep experiments.

X-ray Scattering. Simultaneous small angle (SAXS), mid angle (MAXS) and wide angle (WAXS) x-ray scattering data were collected at beamline 5-ID-D at the Advance Photon Source using a

triple area detector system. The SAXS detector (6 x 6 binning) is a four-module charge coupled device (CCD) while the MAXS (4 x 4 binning) and WAXS (2 x 2 binning) detectors are a two module CCD, all from Rayonix LLC. The direct beam position and detector distances were calibrated using lanthanum hexaboride (WAXS at 0.2 m), silver behenate (MAXS at 1.0 m) and a silicon diffraction grating (SAXS at 8.5 m). Scattering intensities were calibrated using a glassy carbon standard. The data were collected along the center axis of each sample at x-ray energies of 17 keV and a wavelength of 0.7293 Å that resulted in q-ranges from 2.54 x 10^{-3} to 4.5 $Å^{-1}$. [49, 62] The PDMS-NH_3^+PSS nanoparticle dispersion was prepared using FNP and filtered through a 0.1 µm filter and concentrated at room temperature to 1 wt%. The PDMS-NH_3^+PSS nanocomposite was prepared as above and dried at 100 ºC under vac for 24 h. The water, PSS, PDMS-NH_2, PDMS-$NH_3^+Tf^-$ and PDMS-NH_3^+PSS dispersions were transferred into 1.5 mm thin-wall fused silica capillary tubes. For all solution samples, the capillary was in motion at 0.508 mm/sec whereas the nanocomposite was stationary.[49, 62]

X-ray Data Analysis. SAXS/MAXS/WAXS data were averaged and the water background was subtracted using RAW.[63] Data modeling and analysis were performed using the IRENA 2.7 package for Igor Pro 8.04. Particle properties were determined using a unified Guinier exponential and power law fit.[51, 58, 64, 65]

UV-VIS Absorbance. The sorption of 2-(furan-2-yl)-3-hydroxy-4H-chromen-4-one (FG38) 5 x 10^{-6} M in water into a 1:1 PSS: PDMS-NH_3^+ nanocomposite was monitored at 358 nm over a 24 h period using a UV-Vis spectrometer. The absorbance of FG38 in water was plotted vs. time (Figure S16).

Fluorescence and Lifetime Measurements. The emission spectra of FG38 in water (5 x 10^{-6} M) and in the PDMS-NH_3^+PSS nanocomposite were recorded using an Edinburgh 298 FS5 steady-state spectrometer. Using a 150 W xenon lamp, the samples were excited at a wavelength of 360 nm. Time-correlated single photon counting (TCSPC) was used to measure the emission decay

lifetime. The excitation source was an Edinburgh EPL-365 ps pulsed diode laser. The emission counts were monitored at 543 nm and 430 nm, and the data was collected to 10000 counts. The decay lifetimes were fit using a biexponential fit.

ASSOCIATED CONTENT

Supporting Information

The Supporting Information is available free of charge at

COSY ^{1}H NMR and ^{1}H NMR of PDMS-NH_2 and PDMS-$NH_3^+Tf^-$; details of flash nanoprecipitation mixer; DLS of PDMS-$NH_3^+Tf^-$ and PDMS-NH_3^+PSS nanoparticles showing stability; DLS showing optimization of ratio of PSS to polysiloxane; DLS showing stability of nanoparticles in 0.15 M NaCl; UV-vis spectrum of PSS remaining in solution after nanoparticle formation; FTIR of PDMS-NH_3^+PSS nanoparticles showing residual Tf^- ion; viscosity *versus* frequency of PDMS-NH_3^+PSS nanocomposite and bulk PDMS-$NH_3^+Tf^-$; WAXS profile of water scattering region; SAXS profiles showing the contribution of each population in PDMS-NH_3^+PSS nanoparticle suspension in water, PDMS-NH_3^+PSS nanocomposite and bulk PDMS-$NH_3^+Tf^-$; x-ray scattering profile of PSS in water showing the “polyelectrolyte peak”; AFM of PDMS-NH_3^+PSS nanoparticles deposited on Si wafer; Table containing detailed SAXS fit parameters; UV-vis absorption spectrum of FG38 in water; kinetics of FG38 sorption by PDMS-NH_3^+PSS nanocomposite; emission decay curves of FG38 in PDMS-NH_3^+PSS nanocomposite.

AUTHOR INFORMATION

Corresponding Author

Joseph B. Schlenoff, Department of Chemistry and Biochemistry, The Florida State University, Tallahassee, FL 32308 USA

10.1021/acs.langmuir.2c01019

Authors

Sandrine Lteif, Department of Chemistry and Biochemistry, The Florida State University, Tallahassee, FL 32308 USA

Khalil Akkaoui, Department of Chemistry and Biochemistry, The Florida State University, Tallahassee, FL 32308 USA

Samir Abou Shaheen, Department of Chemistry and Biochemistry, The Florida State University, Tallahassee, FL 32308 USA

Maya Chaaban, Department of Chemistry and Biochemistry, The Florida State University, Tallahassee, FL 32308 USA

Steven Weigand, DND-CAT Synchrotron Research Center, Northwestern University, APS/ANL 432-A005, 9700 S. Cass Avenue, Argonne, Illinois 60439, USA

Author Contributions

The manuscript was written through contributions of all authors. All authors have given approval to the final version of the manuscript.

Notes

The authors declare no competing financial interest.

ACKNOWLEDGMENTS

The authors are grateful for support provided by the National Science Foundation (DMR 1809304 and DMR 2103703). Portions of this work were performed at the DuPont-Northwestern-Dow Collaborative Access Team (DND-CAT) located at Sector 5 of the Advanced Photon Source (APS). DND-CAT is supported by Northwestern University, The Dow Chemical Company, and DuPont de Nemours, Inc. This research used resources of the Advanced Photon Source, a U.S.

Department of Energy (DOE) Office of Science User Facility operated for the DOE Office of Science by Argonne National Laboratory under Contract No. DE-AC02-06CH11357. Data was collected using an instrument funded by the National Science Foundation under Award Number 0960140.

REFERENCES

1. Jancar, J.; Douglas, J.; Starr, F. W.; Kumar, S.; Cassagnau, P.; Lesser, A.; Sternstein, S. S.; Buehler, M., Current Issues in Research on Structure–Property Relationships in Polymer Nanocomposites. *Polymer* **2010,** *51*, 3321-3343.

2. Senses, E.; Tyagi, M.; Pasco, M.; Faraone, A., Dynamics of Architecturally Engineered All-Polymer Nanocomposites. *ACS Nano* **2018,** *12*, 10807-10816.

3. Genix, A.-C.; Bocharova, V.; Kisliuk, A.; Carroll, B.; Zhao, S.; Oberdisse, J.; Sokolov, A. P., Enhancing the Mechanical Properties of Glassy Nanocomposites by Tuning Polymer Molecular Weight. *ACS App. Mat. Interfaces* **2018,** *10*, 33601-33610.

4. Kao, J.; Thorkelsson, K.; Bai, P.; Rancatore, B. J.; Xu, T., Toward Functional Nanocomposites: Taking the Best of Nanoparticles, Polymers, and Small Molecules. *Chem. Soc. Rev.* **2013,** *42*, 2654-2678.

5. Kumar, S. K.; Benicewicz, B. C.; Vaia, R. A.; Winey, K. I., 50th Anniversary Perspective: Are Polymer Nanocomposites Practical for Applications? *Macromolecules* **2017,** *50*, 714-731.

6. Wang, Y.; Yu, Z.; Dufresne, A.; Ye, Z.; Lin, N.; Zhou, J., Quantitative Analysis of Compatibility and Dispersibility in Nanocellulose-Reinforced Composites: Hansen Solubility and Raman Mapping. *ACS Nano* **2021,** *15*, 20148-20163.

7. Crosby, A. J.; Lee, J. Y., Polymer Nanocomposites: The “Nano” Effect on Mechanical Properties. *Polym. Rev.* **2007,** *47*, 217-229.

8. Molero, G.; Liu, C.; Zhu, Z.; Chen, Q.; Peterson, S. R.; Kolluru, P. V.; Sue, H.-J.; Uenuma, S.; Mayumi, K.; Ito, K., Fracture Behavior of Polyrotaxane-Toughened Poly(Methyl Methacrylate). *Langmuir* **2022,** *38*, 2335-2345.

9. Semenova, A.; Vidallon, M. L. P.; Follink, B.; Brown, P. L.; Tabor, R. F., Synthesis and Characterization of Polyethylenimine–Silica Nanocomposite Microparticles. *Langmuir* **2022,** *38*, 191-202.

10. Schmarsow, R. N.; dell'Erba, I. E.; Villaola, M. S.; Hoppe, C. E.; Zucchi, I. A.; Schroeder, W. F., Effect of Light Intensity on the Aggregation Behavior of Primary Particles During in Situ Photochemical Synthesis of Gold/Polymer Nanocomposites. *Langmuir* **2020,** *36*, 13759-13768.

11. Larsson, P. A.; Berglund, L. A.; Wågberg, L., Ductile All-Cellulose Nanocomposite Films Fabricated from Core–Shell Structured Cellulose Nanofibrils. *Biomacromolecules* **2014,** *15*, 2218-2223.

12. Huo, Y.; Liu, Y.; Yang, J.; Du, H.; Qin, C.; Liu, H., Polydopamine-Modified Cellulose Nanofibril Composite Aerogel: An Effective Dye Adsorbent. *Langmuir* **2022,** *38*, 4164-4174.

13. Kozakiewicz, J.; Ofat, I.; Trzaskowska, J., Silicone-Containing Aqueous Polymer Dispersions with Hybrid Particle Structure. *Adv. Colloid and Interface Sci.* **2015,** *223*, 1-39.

14. Knauert, S. T.; Douglas, J. F.; Starr, F. W., The Effect of Nanoparticle Shape on Polymer-Nanocomposite Rheology and Tensile Strength. *J. Polym. Sci. B Polym. Phys.* **2007,** *45*, 1882-1897.

15. Liu, D.; Song, L.; Song, H.; Chen, J.; Tian, Q.; Chen, L.; Sun, L.; Lu, A.; Huang, C.; Sun, G., Correlation between Mechanical Properties and Microscopic Structures of an Optimized Silica Fraction in Silicone Rubber. *Compos. Sci. Technol.* **2018,** *165*, 373-379.

16. Zhao, M.; Baker, J.; Jiang, Z.; Zhu, Z.; Wu, H.-M.; Wu, J.-L.; Kang, W.-H.; Sue, H.-J., Preparation of Well-Exfoliated Poly(Ethylene-co-Vinyl Acetate)/A-Zirconium Phosphate Nanocomposites. *Langmuir* **2021,** *37*, 4550-4561.

17. Han, J.; Liang, Y.; He, C.; Tong, Y.; Li, W., Porous PVA-G-SPA/PVA-SA Catalytic Composite Membrane Via Lyophilization for Esterification Enhancement. *Langmuir* **2022,** *38*, 2660-2667.

18. Rao, J. P.; Geckeler, K. E., Polymer Nanoparticles: Preparation Techniques and Size-Control Parameters. *Prog. Polym. Sci.* **2011,** *36*, 887-913.

19. Owen, S. C.; Chan, D. P.; Shoichet, M. S., Polymeric Micelle Stability. *Nano Today* **2012,** *7*, 53-65.

20. Zhao, W.; Fonsny, P.; FitzGerald, P.; Warr, G. G.; Perrier, S., Unexpected Behavior of Polydimethylsiloxane/Poly (2-(Dimethylamino) Ethyl Acrylate)(Charged) Amphiphilic Block Copolymers in Aqueous Solution. *Polym. Chem.* **2013,** *4*, 2140-2150.

21. Maparu, A. K.; Singh, P.; Rai, B.; Sharma, A.; Sivakumar, S., Stable Sub-100 nm PDMS Nanoparticles as an Intracellular Drug Delivery Vehicle. *Mater. Sci. Eng. C* **2021,** *119*, 111577.

22. Ge, M.; Cao, C.; Liang, F.; Liu, R.; Zhang, Y.; Zhang, W.; Zhu, T.; Yi, B.; Tang, Y.; Lai, Y., A “PDMS-in-Water” Emulsion Enables Mechanochemically Robust Superhydrophobic Surfaces with Self-Healing Nature. *Nanoscale Horiz.* **2020,** *5*, 65-73.

23. Car, A.; Baumann, P.; Duskey, J. T.; Chami, M.; Bruns, N.; Meier, W., pH-Responsive PDMS-b-PDMAEMA Micelles for Intracellular Anticancer Drug Delivery. *Biomacromolecules* **2014,** *15*, 3235-3245.

24. Peng, J.; Tomsia, A. P.; Jiang, L.; Tang, B. Z.; Cheng, Q., Stiff and Tough PDMS-MMT Layered Nanocomposites Visualized by AIE Luminogens. *Nat. Comm.* **2021,** *12*, 1-9.

25. Fu, F. S.; Mark, J., Elastomer Reinforcement from a Glassy Polymer Polymerized in Situ. *J. Polym. Sci. B Polym. Phys.* **1988,** *26*, 2229-2235.

26. Shen, L.; Wang, T.-p.; Goyal, S.; Lee, T.-H.; Lin, F.-Y.; Torres, S.; Robison, T.; Cochran, E. W., Easy-Processable and Aging-Free All-Polymer Polysiloxane Composites. *ACS App. Polym. Mater.* **2020,** *2*, 5835-5844.

27. Hossen, S.; Hossain, M. K.; Basher, M.; Mia, M.; Rahman, M.; Uddin, M. J., Smart Nanocarrier-Based Drug Delivery Systems for Cancer Therapy and Toxicity Studies: A Review. *J. Adv. Res.* **2019,** *15*, 1-18.

28. Krajangpan, S.; Kalita, H.; Chisholm, B. J.; Bezbaruah, A. N., Iron Nanoparticles Coated with Amphiphilic Polysiloxane Graft Copolymers: Dispersibility and Contaminant Treatability. *Environmental Science & Technology* **2012,** *46*, 10130-10136.

29. Ge, J.; Ye, Y.-D.; Yao, H.-B.; Zhu, X.; Wang, X.; Wu, L.; Wang, J.-L.; Ding, H.; Yong, N.; He, L.-H.; Yu, S.-H., Pumping through Porous Hydrophobic/Oleophilic Materials: An Alternative Technology for Oil Spill Remediation. *Angewandte Chemie International Edition* **2014,** *53*, 3612-3616.

30. Saad, W. S.; Prud'homme, R. K., Principles of Nanoparticle Formation by Flash Nanoprecipitation. *Nano Today* **2016,** *11*, 212-227.

31. Han, J.; Zhu, Z.; Qian, H.; Wohl, A. R.; Beaman, C. J.; Hoye, T. R.; Macosko, C. W., A Simple Confined Impingement Jets Mixer for Flash Nanoprecipitation. *J. Pharm. Sci.* **2012,** *101*, 4018-23.

32. Zhang, C.; Pansare, V. J.; Prud'homme, R. K.; Priestley, R. D., Flash Nanoprecipitation of Polystyrenenanoparticles. *Soft Matter* **2012,** *8*, 86-93.

33. Levit, S. L.; Walker, R. C.; Tang, C., Rapid, Single-Step Protein Encapsulation Via Flash Nanoprecipitation. *Polymers* **2019,** *11*, 1406.

34. Johnson, B. K.; Prud'homme, R. K., Chemical Processing and Micromixing in Confined Impinging Jets. *AIChE Journal* **2003,** *49*, 2264-2282.

35. Mishra, G.; Bhattacharyya, S.; Bhatia, V.; Ateeq, B.; Sharma, A.; Sivakumar, S., Direct Intranuclear Anticancer Drug Delivery Via Polydimethylsiloxane Nanoparticles: In Vitro and in Vivo Xenograft Studies. *ACS App. Mater. Interfaces* **2017,** *9*, 34625-34633.

36. Neumann, B.; Vincent, B.; Krustev, R.; Müller, H.-J., Stability of Various Silicone Oil/Water Emulsion Films as a Function of Surfactant and Salt Concentration. *Langmuir* **2004,** *20*, 4336-4344.

37. Tadros, T., Colloid and Interface Aspects of Pharmaceutical Science. In *Colloid Interf. Sci. Pharm. Res. Development*, Elsevier: 2014; pp 29-54.

38. Gambinossi, F.; Mylon, S. E.; Ferri, J. K., Aggregation Kinetics and Colloidal Stability of Functionalized Nanoparticles. *Adv. Colloid Interf. Sci.* **2015,** *222*, 332-349.

39. Mori, H.; Müller, A. H.; Klee, J. E., Intelligent Colloidal Hybrids Via Reversible pH-Induced Complexation of Polyelectrolyte and Silica Nanoparticles. *J. Am. Chem. Soc.* **2003,** *125*, 3712-3713.

40. Mayya, K. S.; Schoeler, B.; Caruso, F., Preparation and Organization of Nanoscale Polyelectrolyte-Coated Gold Nanoparticles. *Adv. Funct. Mater.* **2003,** *13*, 183-188.

41. Chen, Y.; Yang, M.; Schlenoff, J. B., Glass Transitions in Hydrated Polyelectrolyte Complexes. *Macromolecules* **2021,** *54*, 3822-3831.

42. Mueller, R.; Köhler, K.; Weinkamer, R.; Sukhorukov, G.; Fery, A., Melting of PDADMAC/PSS Capsules Investigated with AFM Force Spectroscopy. *Macromolecules* **2005,** *38*, 9766-9771.

43. Yavitt, B. M.; Salatto, D.; Zhou, Y.; Huang, Z.; Endoh, M.; Wiegart, L.; Bocharova, V.; Ribbe, A. E.; Sokolov, A. P.; Schweizer, K. S., Collective Nanoparticle Dynamics Associated with Bridging Network Formation in Model Polymer Nanocomposites. *ACS Nano* **2021,** *15*, 11501–11513.

44. Zhang, L.; Brostowitz, N. R.; Cavicchi, K. A.; Weiss, R., Perspective: Ionomer Research and Applications. *Macromol. React. Eng.* **2014,** *8*, 81-99.

45. Weiss, R.; Zhao, H., Rheological Behavior of Oligomeric Ionomers. *J. Rheol.* **2009,** *53*, 191-213.

46. Eisenberg, A.; Hird, B.; Moore, R. B., A New Multiplet-Cluster Model for the Morphology of Random Ionomers. *Macromolecules* **1990,** *23*, 4098-4107.

47. Kim, J.-S.; Nishida, M.; Eisenberg, A., Morphology of Sulfonated Random Ionomers Based on Hydrogenated Styrene–Butadiene Copolymer Studied by SAXS. *Polym J* **1999,** *31*, 96-98.

48. Enokida, J. S.; Hu, W.; Fang, H.; Morgan, B. F.; Beyer, F. L.; Winter, H. H.; Coughlin, E. B., Modifying the Structure and Dynamics of Ionomers through Counterion Sterics. *Macromolecules* **2020,** *53*, 1767-1776.

49. Weigand, S. J.; Keane, D. T., DND-CAT's New Triple Area Detector System for Simultaneous Data Collection at Multiple Length Scales. *Nucl. Instrum. Methods Phys. Res. A: Accelerators, Spectrometers, Detectors and Associated Equipment* **2011,** *649*, 61-63.

50. Nishida, K.; Kaji, K.; Kanaya, T., High Concentration Crossovers of Polyelectrolyte Solutions. *J. Chem. Phys.* **2001,** *114*, 8671-8677.

51. Beaucage, G., Approximations Leading to a Unified Exponential/Power-Law Approach to Small-Angle Scattering. *J. Appl. Crystallogr.* **1995,** *28*, 717-728.

52. Bahloul, W.; Bounor-Legaré, V.; David, L.; Cassagnau, P., Morphology and Viscoelasticity of PP/TiO_2 Nanocomposites Prepared by in Situ Sol–Gel Method. *Journal of Polymer Science Part B: Polymer Physics* **2010,** *48*, 1213-1222.

53. Beaucage, G.; Ulibarri, T.; Black, E.; Schaefer, D. In *Multiple Size Scale Structures in Silica-Siloxane Composites Studied by Small-Angle Scattering*, ACS Symposium Series, Washington, DC: American Chemical Society,[1974]-: 1995; pp 97-111.

54. Beaucage, G., Determination of Branch Fraction and Minimum Dimension of Mass-Fractal Aggregates. *Phys. Rev. E* **2004,** *70*, 031401.

55. Amann, M.; Diget, J. S.; Lyngsø, J.; Pedersen, J. S.; Narayanan, T.; Lund, R., Kinetic Pathways for Polyelectrolyte Coacervate Micelle Formation Revealed by Time-Resolved Synchrotron SAXS. *Macromolecules* **2019,** *52*, 8227-8237.

56. McGlasson, A.; Rishi, K.; Beaucage, G.; Chauby, M.; Kuppa, V.; Ilavsky, J.; Rackaitis, M., Quantification of Dispersion for Weakly and Strongly Correlated Nanofillers in Polymer Nanocomposites. *Macromolecules* **2020,** *53*, 2235-2248.

57. Zhao, J.; Chen, P.; Lin, Y.; Chang, J.; Lu, A.; Chen, W.; Meng, L.; Wang, D.; Li, L., Stretch-Induced Crystallization and Phase Transitions of Poly (Dimethylsiloxane) at Low Temperatures: An in Situ Synchrotron Radiation Wide-Angle X-Ray Scattering Study. *Macromolecules* **2018,** *51*, 8424-8434.

58. Mircea Anitas, E., Small-Angle Scattering from Weakly Correlated Nanoscale Mass Fractal Aggregates. *Nanomaterials* **2019,** *9*, 648.

59. Gao, F.; Dharia, J. R.; McGowan, W. M.; Hiliski, E. F.; Johnson, K. F.; Schlenoff, J. B., Novel Proton-Transfer Fluors Based in 3-Hydroxyflavone. In *Scifi93 Workshop on Scintillating Fiber Detectors*, Bross, A. D.; Richti, R. C.; Wayne, M., Eds. World Scientific: Singapore, 1995; pp 361-368.

60. Das, R.; Duportail, G.; Richert, L.; Klymchenko, A.; Mély, Y., Sensing Micelle Hydration by Proton-Transfer Dynamics of a 3-Hydroxychromone Dye: Role of the Surfactant Headgroup and Chain Length. *Langmuir* **2012,** *28*, 7147-7159.

61. Decher, G., Fuzzy Nanoassemblies: Toward Layered Polymeric Multicomposites. *Science* **1997,** *277*, 1232-1237.

62. Weigand, S.; Stillwell, B.; Guise, W. E.; Quintana, J. P.; Keane, D. T., Flexibility and High Throughput: Supporting Saxs Users at a Joint Industrial Academic Beamline. *Adv. X-Ray Anal* **2009,** *52*, 58-68.

63. Hopkins, J. B.; Gillilan, R. E.; Skou, S., Bioxtas Raw: Improvements to a Free Open-Source Program for Small-Angle X-Ray Scattering Data Reduction and Analysis. *J. App. Crystallogr.* **2017,** *50*, 1545-1553.

64. Nelson, A., Co-Refinement of Multiple-Contrast Neutron/X-Ray Reflectivity Data Using Motofit. *J. App. Crystallogr.* **2006,** *39*, 273-276.

65. Ilavsky, J.; Jemian, P. R., IRENA: Tool Suite for Modeling and Analysis of Small-Angle Scattering. *J. App. Crystallogr.* **2009,** *42*, 347-353.

TOC GRAPHIC for publication only